Structural properties of hyperuniform Voronoi networks

Eli Newby [1], Wenlong Shi [2], Yang Jiao [2,3,*], Reka Albert [1,†] and Salvatore Torquato [4,5,6,7,‡]

[1]*Department of Physics, Pennsylvania State University University Park, Pennsylvania 16802, USA*
[2]*Materials Science and Engineering, Arizona State University, Tempe, Arizona 85287, USA*
[3]*Department of Physics, Arizona State University, Tempe, Arizona 85287, USA*
[4]*Department of Chemistry, Princeton University, Princeton, New Jersey 08544, USA*
[5]*Department of Physics, Princeton University, Princeton, New Jersey 08544, USA*
[6]*Princeton Institute of Materials, Princeton University, Princeton, New Jersey 08544, USA*
[7]*Program in Applied and Computational Mathematics, Princeton University, Princeton, New Jersey 08544, USA*

(Received 10 November 2024; accepted 3 March 2025; published 20 March 2025)

Disordered hyperuniform many-particle systems are recently discovered exotic states of matter, characterized by the complete suppression of normalized infinite-wavelength density fluctuations, as in perfect crystals, while lacking conventional long-range order, as in liquids and glasses. In this work, we begin a program to quantify the structural properties of nonhyperuniform and hyperuniform networks. In particular, large two-dimensional (2D) Voronoi networks (graphs) containing approximately 10,000 nodes are created from a variety of different point configurations, including the antihyperuniform hyperplane intersection process (HIP), nonhyperuniform Poisson process, nonhyperuniform random sequential addition (RSA) saturated packing, and both non-stealthy and stealthy hyperuniform point processes. We carry out an extensive study of the Voronoi-cell area distribution of each of the networks by determining multiple metrics that characterize the distribution, including their average areas and corresponding variances as well as higher-order cumulants (i.e., skewness γ_1 and excess kurtosis γ_2). We show that the HIP distribution is far from Gaussian, as evidenced by a high skewness ($\gamma_1 = 3.16$) and large positive excess kurtosis ($\gamma_2 = 16.2$). The Poisson (with $\gamma_1 = 1.07$ and $\gamma_2 = 1.79$) and non-stealthy hyperuniform (with $\gamma_1 = 0.257$ and $\gamma_2 = 0.0217$) distributions are Gaussian-like distributions, since they exhibit a small but positive skewness and excess kurtosis. The RSA (with $\gamma_1 = 0.450$ and $\gamma_2 = -0.0384$) and the highest stealthy hyperuniform distributions (with $\gamma_1 = 0.0272$ and $\gamma_2 = -0.0626$) are also non-Gaussian because of their low skewness and negative excess kurtosis, which is diametrically opposite of the non-Gaussian behavior of the HIP. The fact that the cell-area distributions of large, finite-sized RSA and stealthy hyperuniform networks (e.g., with $N \approx 10,000$ nodes) are narrower, have larger peaks, and smaller tails than a Gaussian distribution implies that in the thermodynamic limit the distributions should exhibit compact support, consistent with previous theoretical considerations. Moreover, we compute the Voronoi-area correlation functions $C_{00}(r)$ for the networks, which describe the correlations between the area of two Voronoi cells separated by a given distance r [M. A. Klatt and S. Torquato, Phys. Rev. E **90**, 052120 (2014)]. We show that the correlation functions $C_{00}(r)$ qualitatively distinguish the antihyperuniform, nonhyperuniform, and hyperuniform Voronoi networks considered here. Specifically, the antihyperuniform HIP networks possess a slowly decaying $C_{00}(r)$ with large positive values, indicating large fluctuations of Voronoi cell areas across scales. While the nonhyperuniform Poisson and RSA network possess positive and fast decaying $C_{00}(r)$, we find strong anticorrelations in $C_{00}(r)$ (i.e., negative values) for the hyperuniform networks. The latter indicates that the large-scale area fluctuations are suppressed by accompanying large Voronoi cells with small cells (and vice versa) in the systems in order to achieve hyperuniformity. In summary, we have shown that cell-area distributions and pair correlation functions of Voronoi networks enable one to distinguish quantitatively antihyperuniform, standard nonhyperuniform, and hyperuniform networks from one another.

DOI: 10.1103/PhysRevE.111.034123

I. INTRODUCTION

Disordered hyperuniform many-particle systems in d-dimensional Euclidean space $\mathbb{R}^d$ are exotic amorphous states in which the normalized density fluctuations are completely suppressed at infinite wavelengths [1,2]. In the last two decades, such disordered systems have been shown to arise in a variety of contexts in the physical, mathematical, and biological sciences [1–23]. Disordered hyperuniform materials have received great attention because they possess many unique optical, mechanical, and transport properties [24–39].

A *hyperuniform* system, disordered or not, can be defined in two equivalent ways. A hyperuniform many-particle system

*Contact author: yang.jiao.2@asu.edu
†Contact author: rza1@psu.edu
‡Contact author: torquato@electron.princeton.edu

 ©2025 American Physical Society

is one in which the number variance of particles within a spherical observation window of radius R grows slower than the observation window volume R^d for large R [1,2], i.e.,

$$\lim_{R\to\infty} \sigma_N^2(R)/v_1(R) = 0 \tag{1}$$

where $\sigma_N^2(R) \equiv \langle N(R)^2\rangle - \langle N(R)\rangle^2$ is the variance in the number of points (brackets indicate the ensemble average), and $v_1(R) \sim R^d$ is the volume of a d-dimensional sphere of radius R. Equivalently, a many-particle system is hyperuniform if its structure factor $S(\mathbf{k})$ tends to zero as the wavenumber $k \equiv |\mathbf{k}|$ tends to zero, i.e.,

$$\lim_{|\mathbf{k}|\to 0} S(\mathbf{k}) = 0. \tag{2}$$

The small-k scaling behavior of $S(k) \sim k^\alpha$ determines the large-R asymptotic behavior of $\sigma_N^2(R)$, based on which all hyperuniform systems, disordered or not, can be categorized into three classes: $\sigma_N^2(R) \sim R^{d-1}$ for $\alpha > 1$ (class I); $\sigma_N^2(R) \sim R^{d-1}\ln(R)$ for $\alpha = 1$ (class II); and $\sigma_N^2(R) \sim R^{d-\alpha}$ for $0 < \alpha < 1$ (class III) [2]. Consequently, hyperuniform systems encompass all crystals and quasicrystals [1,2]. A special subset of class-I hyperuniform systems possess a zero structure factor for a range of wavenumbers around the origin, i.e., $S(k) = 0$ for $k < K^*$ (excluding the forward scattering), which are referred to as stealthy hyperuniform systems. Stealthy hyperuniform systems include all crystals and certain special disordered systems, which are characterized by a parameter $\chi \in (0, 0.5)$ reflecting the fraction of the constrained degrees of freedom in the system [40–43], see Sec. II for more details. Increasing χ also leads to an increase of the local order in the system.

Although this exotic state of matter continues to be identified in more fields and their unique properties are being further illuminated, the preponderance of previous work has focused on hyper decipherable uniform particle configurations, two-phase media, and random fields [1,2,4,6]. On the other hand, only a few studies have been carried out on hyperuniform networks [44,45]. Here, we focus on the "spatial networks" derived from point configurations, i.e., graphs whose nodes are embedded in a space with a metric (e.g., a Euclidean space distance) [46,47]. In particular, we construct networks using the Voronoi tessellations of point patterns [48–50].

A Voronoi tessellation in 2D is a partition of the plane by convex polygonal cells, which are referred to as Voronoi cells [49]. The Voronoi cell associated with a point is defined to be the region of space nearer to this point than to any other point in the point pattern (see Sec. II B for details). We convert the tessellation into a network by specifying the vertices of the Voronoi polygons as nodes and the edges of the polygons as edges of the network. We note that there are multiple ways of converting a point pattern into a spatial network [51–56], and each was found to have both pros and cons. We choose Voronoi networks because such networks are widely applied in numerous different fields, including biology, meteorology, metallurgy, crystallography, forestry, ecology, archaeology, geology, geography, astrophysics, physics, computer science, and engineering [49]. Moreover, previous theoretical studies have established analytical results for such systems that can be used as benchmarks for our current study [41,57].

We comprehensively analyze the networks constructed from the Voronoi tessellation of the point patterns. First, we perform an analysis of the area distribution of Voronoi cells to recapitulate previously found results regarding the size of holes in the point pattern [43,58–61]. In particular, we calculate the the first four cumulants, including average $\bar{A}$, variance σ_A^2, skewness γ_1 and excess kurtosis γ_2 associated with the Voronoi-cell area distributions of large, finite-sized two-dimensional systems containing $N \approx 10,000$ points built from hyperplane intersection process (HIP) [62], Poisson, random sequential addition (RSA) [57,63], and both non-stealthy hyperuniform [61,64] and stealthy hyperuniform [40,65,66] point processes. The higher-order cumulants of each distribution reveal the shape of the cell-area distribution, and they compare the probability density function to a Gaussian distribution (i.e., $\gamma_1 = 0$, $\gamma_2 = 0$). The n^{th} cumulant κ_n of a distribution is defined as the n^{th} derivative of the cumulant-generating function evaluated at 0, i.e., $\kappa_n = K^{(n)}(0)$. The cumulant-generating function is defined as $K(t) = \log \mathbb{E}[e^{tx}]$, where X is the distribution of Voronoi cell areas and $\mathbb{E}$ is the expected value function. Thus, the first cumulant is the mean, the second cumulant is variance, and the higher-order third and fourth moments are related to the skewness and kurtosis of the distribution, respectively.

Our analysis reveals that the Poisson and non-stealthy hyperuniform cell-area distributions are Gaussian-like because they possess small, positive skewness and excess kurtosis values (i.e., $\gamma_1 = 1.07,\ 0.257$, and $\gamma_2 = 1.79,\ 0.0217$ for the Poisson and non-stealthy hyperuniform distributions respectively). In contrast, the antihyperuniform HIP system has a large positive skewness ($\gamma_1 = 3.16$) and excess kurtosis ($\gamma_2 = 16.2$), indicating it is far from Gaussian. The RSA and high-χ stealthy hyperuniform systems are also non-Gaussian because they have low skewness and negative excess kurtosis (i.e., $\gamma_1 = 0.450,\ 0.0492,\ 0.0272$, and $\gamma_2 = -0.0383,\ -0.119,\ -0.0626$ for the RSA, stealthy $\chi = 0.40$, and stealthy $\chi = 0.49$ respectively), yet they possess non-Gaussian behavior diametrically opposite of the HIP systems. Moreover, the low-χ stealthy hyperuniform systems are not Gaussian-like because they are also very peaked and their right tail decreases faster than a Gaussian curve. However, this is not directly decipherable from their skewness and excess kurtosis values due to a left tail in their distributions.

We note that the Voronoi networks analyzed here are necessarily finite in size, even if relatively large with $N \approx 20,000$ nodes. Distributions associated with finite systems will always appear to possess finite support (i.e., a finite subset of the distribution's domain has nonzero frequencies), even if the support becomes infinite (such as a Poisson distribution) in the thermodynamic limit (i.e., $N \to \infty$) [41]. This is because the probability of observing arbitrarily large holes of the order of the system size is vanishingly small. Therefore, in order to correctly ascertain the behaviors of infinite networks, the tail behaviors of the simulated finite-sized distributions are analyzed. Systems possessing infinite support in the thermodynamic limit (e.g., Poisson) can be inferred from an exponential or power-law decaying tail in the distributions associated with sufficiently large, yet finite-sized systems. Similarly, one can infer compact support (i.e., the domain of cell areas that achieve nonzero frequencies is closed and

bounded) for RSA and all stealthy cases from our finite-sized simulations in the same way consistent with the known theoretical results for these models [41,57].

To further characterize the Voronoi networks, we compute the Voronoi-area correlation functions $C_{00}(r)$ for the networks [44]. In particular, $C_{00}(r)$ is defined as the correlation between the volume of two Voronoi cells given that the corresponding centers are separated by distance r (see Sec. II B for details). We observe strong anticorrelations in $C_{00}(r)$ (i.e., negative values) for the hyperuniform networks, consistent with previous analysis of the hyperuniform MRJ sphere packings in 3D [44]. On the other hand, the antihyperuniform HIP networks possess a slowly decaying $C_{00}(r)$ with large positive values, indicating large fluctuations of Voronoi cell areas across scales, while the nonhyperuniform Poisson and RSA network possess positive and much faster decaying $C_{00}(r)$. These results indicate that the large-scale area fluctuations in the hyperuniform networks are effectively suppressed by accompanying large Voronoi cells with small cells (and vice versa), in contrast to the nonhyperuniform networks in which the Voronoi cells with different areas do not possess any notable correlations. To summarize, we find the correlation functions $C_{00}(r)$ qualitatively distinguish the antihyperuniform, nonhyperuniform and hyperuniform Voronoi networks considered here.

The rest of the paper is organized as follows: In Sec. II, we provide definitions of hyperuniformity as well as the Voronoi-area correlation functions. In Sec. III, we present our results, including the comprehensive Voronoi distribution analysis as well as the correlation function analysis of all seven network systems. In Sec. IV, we provide concluding remarks and discuss future directions.

II. DEFINITIONS

A. Structure factor and hyperuniformity

Point configurations in d-dimensional Euclidean space $\mathbb{R}^d$ are fully spatially characterized by an infinite set of n-particle correlation functions $\rho_n(\mathbf{r}_1,\ldots,\mathbf{r}_n)$, which are proportional to the probability of finding n particles at the positions $\mathbf{r}_1,\ldots,\mathbf{r}_n$ [67]. For statistically homogeneous systems, $\rho_1(\mathbf{r}_1)=\rho$, and $\rho_2(\mathbf{r}_1,\mathbf{r}_2)=\rho^2 g_2(\mathbf{r})$, where $\mathbf{r}=\mathbf{r}_1-\mathbf{r}_2$, and $g_2(\mathbf{r})$ is the pair correlation function. If the system is also statistically isotropic, then $g_2(\mathbf{r})=g_2(r)$, where $r=|r|$. The ensemble-averaged structure factor $S(\mathbf{k})$ is defined as

$$S(\mathbf{k})=1+\rho\tilde{h}(\mathbf{k}) \tag{3}$$

where $\tilde{h}(\mathbf{k})$ is the Fourier transform of the total correlation function $h(\mathbf{r})=g_2(\mathbf{r})-1$.

For a single periodic point configuration with N particles at positions $\mathbf{r}^N=(\mathbf{r}_1,\ldots,\mathbf{r}_N)$ within a fundamental cell F of a lattice Λ, the scattering intensity $\mathbb{S}(\mathbf{k})$ is given by

$$\mathbb{S}(\mathbf{k})=\frac{\left|\sum_{j=1}^{N}\exp(-i\mathbf{k}\cdot\mathbf{r}_j)\right|^2}{N}. \tag{4}$$

In the thermodynamic limit, an ensemble of N-particle configurations in F is related to $S(\mathbf{k})$ by

$$\lim_{N,V_F\to\infty}\langle\mathbb{S}(\mathbf{k})\rangle=(2\pi)^d\rho\delta(\mathbf{k})+S(\mathbf{k}), \tag{5}$$

where V_F is the volume of the fundamental cell, and δ is the Dirac delta function [1]. For finite-N simulations under periodic boundary conditions, Eq. 4 is used to compute $S(\mathbf{k})$ directly by averaging over configurations.

Consider systems characterized by a structure factor with a radial power law in the vicinity of the origin,

$$S(\mathbf{k})\sim|\mathbf{k}|^{\alpha}\text{ for }|\mathbf{k}|\to 0. \tag{6}$$

For *hyperuniform* systems, $\alpha>0$, which is referred to as the hyperuniformity exponent. A (standard) *nonhyperuniform* system is one for which $\alpha=0$, i.e., S($\mathbf{k}$) approaches a nonzero constant in the zero-wavenumber limit. An *antihyperuniform* system is one possessing a diverging S($\mathbf{k}$) in the zero-wavenumber limit, i.e., with $\alpha<0$.

For hyperuniform systems, the specific value of α determines large-R scaling behaviors of the number variance [1,2], according to which all hyperuniform systems can be categorized into three different classes:

$$\sigma_N^2(R)\sim\begin{cases}R^{d-1} & \alpha>1,\text{ class I}\\ R^{d-1}\ln(R) & \alpha=1,\text{ class II}\\ R^{d-\alpha} & \alpha<1,\text{ class III.}\end{cases} \tag{7}$$

Classes I and III are the strongest and weakest forms of hyperuniformity, respectively. Class I systems include all crystal structures [1], many quasicrystal structures [68], and exotic disordered systems [4,69]. Examples of class II systems include some quasicrystal structures [68], perfect glasses [70], and maximally random jammed packings [3,71–74]. Examples of class III systems include classical disordered ground states [75], random organization models [76], perfect glasses [70], and perturbed lattices [77]; see Ref. [2] for a more comprehensive list of systems that fall into the three hyperuniformity classes.

Stealthy hyperuniform systems are a special subset of class-I hyperuniform systems possessing a zero structure factor for a range of wavevectors around the origin, i.e.,

$$S(\mathbf{k})=0,\quad\text{for}\quad\mathbf{k}\in\Omega, \tag{8}$$

excluding the forward scattering. Stealthy hyperuniform systems include all crystals and certain special disordered systems, which are characterized by a parameter χ reflecting the fraction of the constrained degrees of freedom in the system [40–43], i.e.,

$$\chi=N_\Omega/(N-d) \tag{9}$$

which is the fraction of constrained degrees of freedom in the systems. We note d degrees of freedom associated with the trivial overall translation of the entire system are subtracted in Eq. (9). In the case of point configurations, it has been shown that increasing χ leads to increased degree of order in the systems [2,66]. Disordered stealthy hyperuniform point configurations can be generated as ground states using the so-called "collective coordinates" approach [41,42,66].

B. Voronoi network and voronoi-area correlation function

A network (or graph) $\mathcal{G}(\mathcal{N},\mathcal{E})$ is defined by a set of nodes $\mathcal{N}$ and its set of connecting M edges $\mathcal{E}$. An edge indicates a local interaction or relationship between a pair of nodes. The

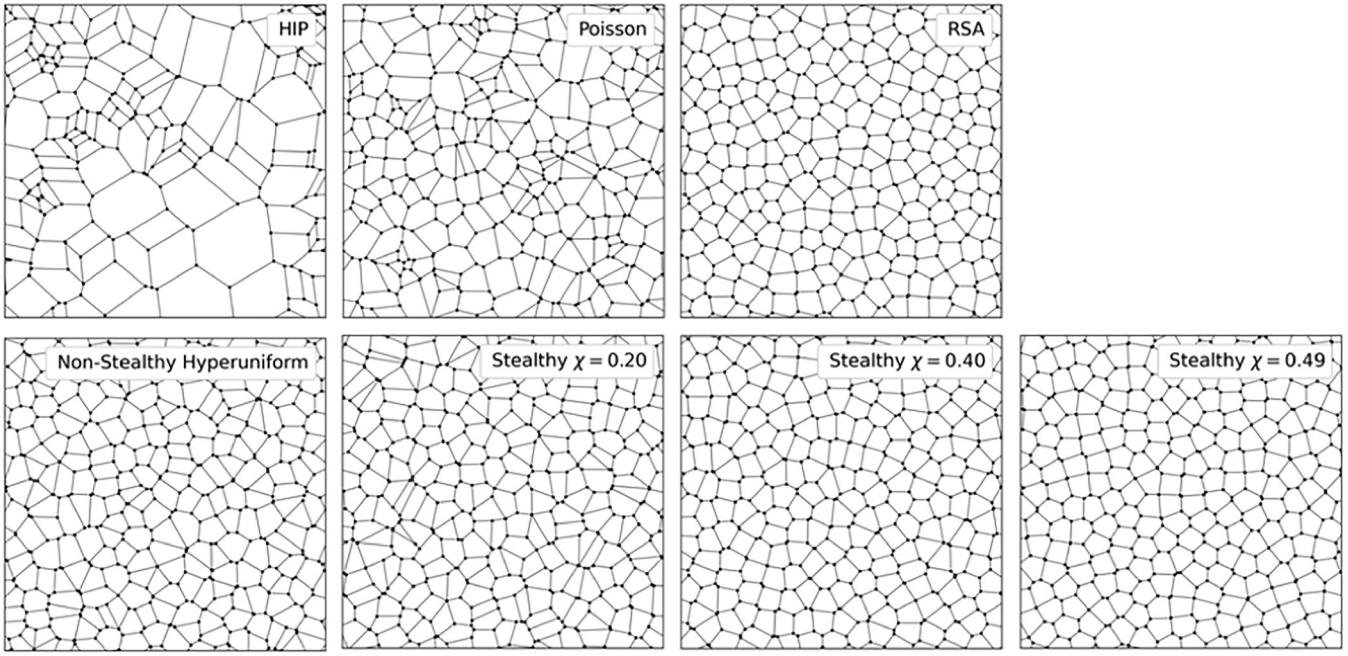


FIG. 1. Snapshot of the Voronoi tessellations of each of the different point processes. The systems in the top row are not hyperuniform, and the systems in the bottom row are hyperuniform.

network is purely defined by the set of nodes and edges, so it can represent an abstraction of the physical system. In this work, we mainly focus on 2D Voronoi networks associated with a configuration of n points $\mathbf{r}_1, \mathbf{r}_2, \ldots, \mathbf{r}_n$ [49]. Associated with the i-th point at $\mathbf{r}_i$ is the Voronoi cell, which is defined to be the region of space nearer to the point at $\mathbf{r}_i$ than to any other point in the set. In two dimensions, such a cell is a convex polygon, and the boundary of the Voronoi polygon is composed of segments of the perpendicular bisectors of each line that connects the point at $\mathbf{r}_i$ to its nearest-neighbor sites (points that share a Voronoi edge). The resulting Voronoi tessellation is then converted to a Voronoi network, by choosing the edges to be the common edge between two Voronoi cells and the nodes to be the common vertices where three cells intersect (i.e., we translate the points of the Voronoi tessellation into nodes and the lines into edges). This allows us to easily compute the area A_i of each Voronoi cell associated with the point at $\mathbf{r}_i$.

Following Ref. [44], we define the Voronoi-area correlation function $C_{00}(\mathbf{r}_1, \mathbf{r}_2)$ as the correlation between the volume of two Voronoi cells given that the corresponding centers are at the positions $\mathbf{r}_1$ and $\mathbf{r}_2$:

$$C_{00}(\mathbf{r}_1, \mathbf{r}_2) = \frac{\langle A(\mathbf{r}_1)A(\mathbf{r}_2)\rangle - \langle A(\mathbf{r}_1)\rangle\langle A(\mathbf{r}_2)\rangle}{\sigma(\mathbf{r}_1|\mathbf{r}_2)\sigma(\mathbf{r}_2|\mathbf{r}_1)} \tag{10}$$

where $\langle\cdot\rangle$ denotes the ensemble average given two points at $\mathbf{r}_1$ and $\mathbf{r}_2$; and $\sigma(\mathbf{r}_i|\mathbf{r}_j)$ is the standard deviation of the area of the Voronoi cell at $\mathbf{r}_i$ given that there is another point at $\mathbf{r}_j$. The conditional variance is defined as $\sigma^2(\mathbf{r}_i|\mathbf{r}_j) = \mathbb{E}((\mathbf{r}_i - \mathbb{E}(\mathbf{r}_i|\mathbf{r}_j))^2|\mathbf{r}_j)$. For a statistically homogeneous and isotropic system, the Voronoi-area correlation is simply a radial function of pair distance r, i.e., $C_{00}(r)$, where $r = |\mathbf{r}_2 - \mathbf{r}_1|$. The function $C_{00}(r) \in [-1, 1]$ measures the correlations, both positive and negative (i.e., anticorrelations), between Voronoi areas of cells given that their centers are at a distance r.

We note that in general, $C_{00}(r)$ does not converge to perfect correlation for vanishing radial distance, i.e., $\lim_{r\to 0} C_{00}(r) < 1$ because for all $r > 1$, $C_{00}(r)$ provides the correlation of two different Voronoi cells with respectively areas $A(0)$ and $A(r)$. On the other hand, because the cell is perfectly correlated with itself, i.e., $C_{00}(r = 0) = 1$, the correlation function $C_{00}(r)$ is discontinuous at the origin. If there is no long-range order, the correlation function tends to zero for infinite radial distance $\lim_{r\to\infty} C_{00}(r) = 0$.

III. RESULTS

We generate the Voronoi tessellations of large, finite-sized two-dimensional systems containing $N \approx 10,000$ points in a large fundamental cell with periodic boundary conditions, which are built from hyperplane intersection process (HIP) [62], Poisson, random sequential addition (RSA) [57,63], and both non-stealthy [61,64] and stealthy [40,65,66] hyperuniform point processes. Figure 1 shows small portions of representative Voronoi networks derived from this diverse set of point configurations. We note that these Voronoi networks are abstractions of the original point configurations and are only defined by their set of nodes and edges. Thus, they do not possess the features that can typically be used to identify hyperuniformity (e.g., the structure factor $S(k)$ as the wavenumber k approaches 0 cannot be directly calculated using the Voronoi networks). We also note that Fig. 1 plots the Voronoi networks, in which the nodes do not directly correspond to the locations of the points in the original point configurations. The structure factor $S(k)$ for the point patterns associated with each Voronoi network is presented in [60,64]. It can be clearly seen that the sizes of Voronoi cells associated with the HIP and Poisson networks

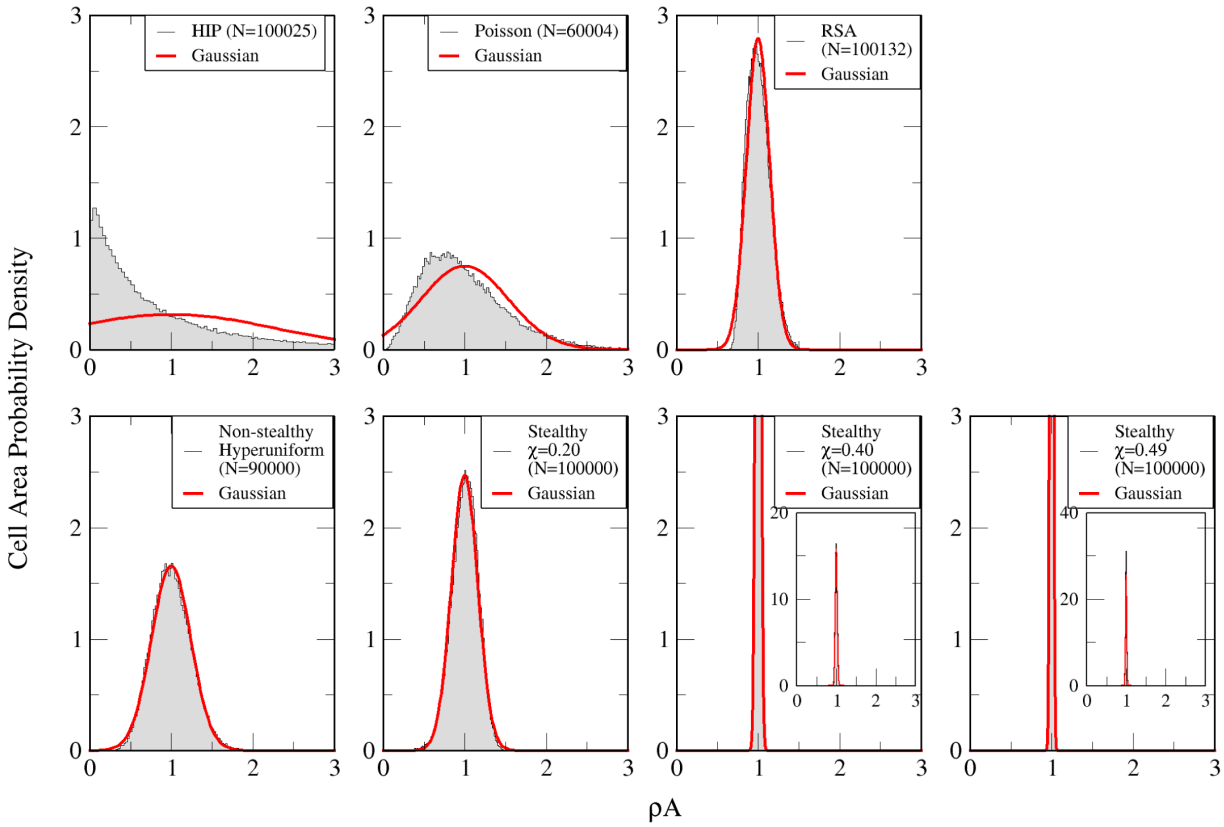


FIG. 2. Graphs of the normalized Voronoi cell-area probability density functions (PDF) calculated from Voronoi tessellations of approximately 10,000 faces associated with various systems. We normalize the cell areas by the density of the system ρ to make the systems comparable to each other. A Gaussian PDF with the same mean and standard deviation is plotted on top of each distribution (red line). To allow for all the distributions to be discernible, we cut off both the x and y axes at 3. For the stealthy $\chi = 0.40$ and $\chi = 0.49$, we include an insert that shows the entire distribution.

fluctuate significantly across the system; while the RSA and hyperuniform networks possess much more uniformly sized Voronoi cells. We note that the areas of Voronoi cells are related to the sizes of holes in the point pattern [41], which is subsequently connected to our current Voronoi network analyses.

A. Voronoi cell-area probability density distributions

We carry out an extensive study of the Voronoi-cell area distribution of each of the networks. Figure 2 shows the normalized Voronoi cell-area probability density functions (PDF) calculated from Voronoi tessellations of approximately 10,000 faces associated with various systems. We normalize the cell areas by the density of the system ρ such that the average area $\bar{A} = 1$ for all systems. A Gaussian PDF with the same mean and standard deviation of the corresponding Voronoi PDF is plotted on top of each distribution (red line). It can be clearly seen that the HIP networks possess PDFs that are distinctly different from the Gaussian distribution, while the other networks' PDFs appear to be well approximated by the Gaussian distribution.

To further quantify the cell-area distributions of the different networks, we compute multiple metrics that characterize the distributions, including the first four cumulants (i.e., average $\bar{A}$, variance σ_A^2, skewness γ_1, and excess kurtosis γ_2) and the information about the domain and range of the cell areas (i.e., the minimum area $A_{\min}$, the maximum area $A_{\max}$, the support $S = A_{\max} - A_{\min}$, the maximum probability density $P_{\max}$). We note that the excess kurtosis of the distribution is indicative of its tail behavior. Positive excess kurtosis indicates stronger tails (decaying slower) than a Gaussian distribution and negative excess kurtosis indicating weaker tails (decaying faster) than a Gaussian. The detailed values of these statistics are provided in Table I.

Consistent with the visual inspection, we find that the antihyperuniform HIP distribution is far from Gaussian, as evidenced by a high skewness ($\gamma_1 = 3.16$) and large positive excess kurtosis ($\gamma_2 = 16.2$). The strong asymmetry of the HIP distribution is mainly due to the excess of large Voronoi cells, associated with the large holes in the system, which also contribute to the large density fluctuations. The HIP distribution also possesses the largest variance $\sigma_A^2 = 1.60$ and support $S = 19.5$ among all systems, indicating the extremely large variations and fluctuations of Voronoi cell sizes in the system.

The Poisson and RSA networks are both standard nonhyperuniform systems. As expected, the uncorrelated Poisson system possesses much larger variance $\sigma_A^2 = 0.283$ and support $S = 5.61$ than the correlated RSA system with $\sigma_A^2 = 0.0204$ and support $S = 1.09$. This indicates that the Voronoi cells in the RSA networks are much more uniform in size, which results from the uniform exclusion volume of the hard

TABLE I. Important statistics of Voronoi cell-area distribution of various systems, including the number of edges M of the Voronoi tessellation, the first four cumulants (i.e., average $\bar{A}$, variance σ_A^2, skewness γ_1, and excess kurtosis γ_2), the information about the domain and range of the cell areas (i.e., the minimum area $A_{\min}$, the maximum area $A_{\max}$, the support $S = A_{\max} - A_{\min}$, the maximum probability density $P_{\max}$ and the detail decay rate λ_R).

	HIP	Poisson	RSA	Non-stealthy hyperuniform	Stealthy $\chi = 0.20$	Stealthy $\chi = 0.40$	Stealthy $\chi = 0.49$
M	100025	60004	100132	90000	100000	100000	100000
$\bar{A}$	1.00	1.00	1.00	1.00	1.00	1.00	1.00
σ_A^2	1.60	0.283	0.0204	0.0580	0.0261	0.000633	0.000240
γ_1	3.16	1.07	0.450	0.257	−0.327	0.0492	0.0272
γ_2	16.2	1.79	−0.0383	0.0217	0.272	−0.119	−0.0626
$A_{\min}$	4.88×10^{-6}	0.0233	0.642	0.212	0.0770	0.896	0.940
$A_{\max}$	19.5	5.64	1.73	2.22	1.57	1.11	1.06
S	19.5	5.61	1.09	2.01	1.50	0.212	0.123
$P_{\max}$	1.27	0.879	2.74	1.68	2.51	16.5	31.1
λ_R	0.237	1.00	9.93	3.93	13.2	57.8	127

disks during the generation of the underlying point patterns. Moreover, the Poisson distribution is Gaussian-like, with a small and positive $\gamma_1 = 1.07$ and $\gamma_2 = 1.79$, except for its cutoff on the left because the area cannot be less than zero. On the other hand, the RSA distribution is non-Gaussian, with $\gamma_1 = 0.450$ and $\gamma_2 = -0.0384$. The negative excess kurtosis indicates a faster-decaying tail than that in a Gaussian distribution. We note that this is distinctly a different non-Gaussian behavior than the HIP distribution. Narrower Voronoi cell-area distribution in the RSA system indicates that it is less likely for the system to contain very large Voronoi cells (and thus, large holes).

Among the hyperuniform networks, the non-stealthy hyperuniform possesses the largest variance $\sigma_A^2 = 0.0580$ and support $S = 2.01$. Both σ_A^2 and support S decrease rapidly (and the peak value $P_{\max}$ increases rapidly) as the degree of hyperuniformity (e.g., quantified via χ) increases. The non-stealthy hyperuniform is also Gaussian-like, possessing small and positive skewness $\gamma_1 = 0.257$ and excess kurtosis $\gamma_2 = 0.0217$, which is consistent with previous result that this system can contain arbitrarily large holes in the thermodynamic limit [64]. On the other hand, the high-χ stealthy hyperuniform distributions (e.g., $\gamma_1 = 0.0272$ and $\gamma_2 = -0.0626$ for $\chi = 0.49$) are also non-Gaussian because of their low skewness and negative excess kurtosis, which is diametrically opposite non-Gaussian behavior of the HIP and indicates the fast decaying tail of the distribution.

B. Analysis of tail behavior of the distributions

The fact that the cell-area distributions of these large, finite-sized RSA and stealthy hyperuniform networks (e.g., with $N \approx 20,000$ nodes) are narrower, have larger peaks, and smaller tails than a Gaussian distribution implies that in the thermodynamic limit these distributions should exhibit compact support, consistent with the previous theoretical considerations [43]. To further illustrate this point, we compare the tail behaviors of the distributions of all systems, which could be used to infer properties of support in the thermodynamic limit. We note that a system with infinite support in the thermodynamic limit possesses a distribution tail that decays at the rate of or slower than an exponential function. This behavior in principle can be captured in the analysis of large, finite-sized realizations as we have here.

In particular, Fig. 3 shows the Voronoi cell-area probability density functions for the different networks on a semi-log plot, which allows us to clearly distinguish the right tail behaviors of the different distributions. It can be clearly seen that the HIP, Poisson, and non-stealthy hyperuniform systems appear to possess a power-law tail, in contrast to the RSA and stealthy systems which appear to decrease (exponentially) faster.

To analyze the tail behavior of these systems, the slope of a linear regression of the end of the right tail is computed to approximate the decay rate of the right tail λ_R, see Table I. To avoid the infinitely negative slope that every distribution must possess because of its finite nature, we measure the slope of the tail slightly before it intersects with the x-axis. While this calculation is only an approximation of decay rate of a non-exponentially decaying distribution, we can use λ_R to observe how the networks decay relative to each other. This is reflected in the λ_R values for our systems with the HIP, Poisson, and

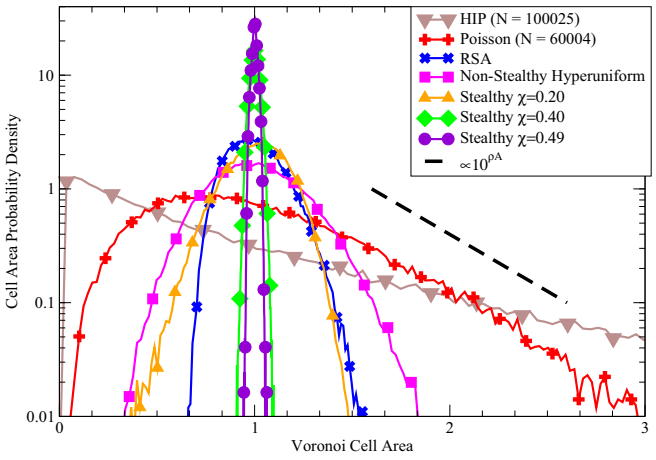


FIG. 3. Voronoi cell-area probability density functions for various system plotted on a semi-log axis. The scaling $\propto 10^{-\rho A}$ is also shown as the dashed line. To allow for all the distributions to be discernible, we cutoff the x axes at 3. For visual clarity, we also only include symbols on every fifth data point.

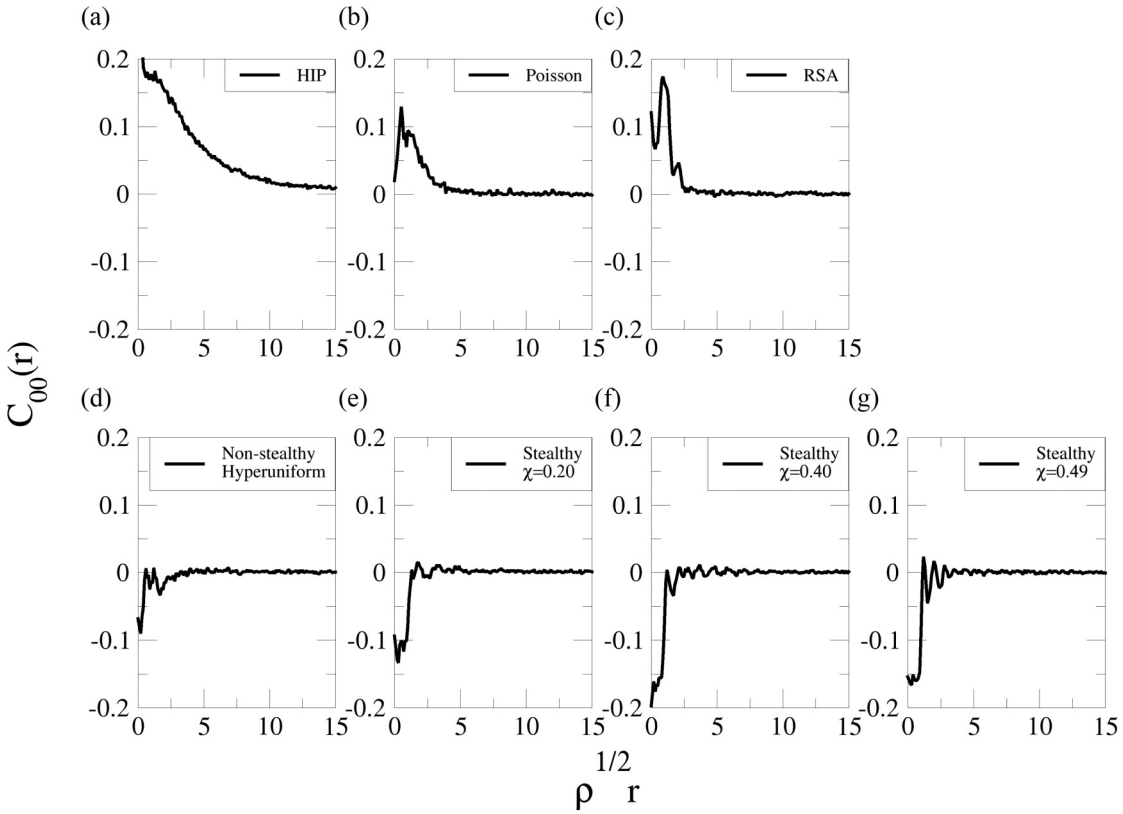


FIG. 4. Voronoi-area correlation functions $C_{00}(r)$ for the antihyperuniform HIP (a), nonhyperuniform Poisson (b) and RSA (c), non-stealthy hyperuniform (d), and stealthy hyperuniform networks with $\chi = 0.2$ (e), $\chi = 0.4$ (f), and $\chi = 0.49$ (g), where r is the distance between the centers of two Voronoi cells and ρ is the number density of the system. All hyperuniform networks exhibit strong anticorrelations in their Voronoi cell areas.

non-stealthy hyperuniform having small decay rates ($\lambda_R = 0.237, 1.00, 3.93$ respectively) while the RSA and stealthy systems have large decay rates ($\lambda_R = 9.93, 13.2, 57.8, 127$ for the RSA, stealthy $\chi = 0.20$, stealthy $\chi = 0.40$, and stealthy $\chi = 0.49$ respectively). From the large λ_R values possessed by the RSA and stealthy systems we can infer that these systems have compact support in the infinite limit. On the other hand, the low λ_R values of the HIP, Poisson, and non-stealthy hyperuniform allow us to infer infinite support for these systems in the thermodynamic limit. Overall, this analysis successfully recapitulates previously known results about these systems and expands on the current knowledge about the geometries of cells of the Voronoi tessellations of various point processes [41,50,65,78–80].

We note that the tail behavior of the Voronoi cell-area distributions is also connected to the hole statistics of the underlying point configurations. In particular, a *hole* in the system of points constitutes a spherical region or radius r that does not contain any points. The void exclusion probability function $E_V(r)$ (i.e., the probability that a hole of size r exists in the infinite system) indicates if an arbitrarily large hole can exist in the system. For example, for an ideal gas of density ρ in two dimensions, the exclusion probability is a decreasing function of r of Gaussian form [49]:

$$E_V(r) = e^{-\rho\pi r^2} \tag{11}$$

Thus, arbitrarily large holes can exist for the ideal gas, even if they have very small probability of occurring. Similarly, it has been found that non-stealthy hyperuniform point patterns allow for arbitrarily large holes [43,81,82]. Conversely, saturated random sequential addition (RSA) and stealthy hyperuniform point patterns have been proven to not tolerate arbitrarily large holes in the thermodynamic limit [43,59].

C. Voronoi-area correlation functions

To further characterize the Voronoi networks of these distinct systems, we compute the Voronoi-area correlation functions $C_{00}(r)$ [44]. Figure 4 shows $C_{00}(r)$ for the antihyperuniform HIP, nonhyperuniform Poisson and RSA, non-stealthy hyperuniform, and stealthy hyperuniform networks. The antihyperuniform HIP networks possess a slowly decaying $C_{00}(r)$ with large positive values. We note that based on the definition (10), larger deviation of $C_{00}(r)$ from 0 indicates larger fluctuations of the Voronoi cell areas. For a Voronoi network with identical cells and orientations (i.e., one derived from a lattice), $C_{00}(r) = 0$ for all r values. Therefore, the large positive values of $C_{00}(r)$ for antihyperuniform HIP networks indicates significant fluctuations of Voronoi cell areas across scales in the system. The nonhyperuniform Poisson and RSA networks also possess a positive $C_{00}(r)$ but with much faster decay.

On the other hand, all hyperuniform networks including both non-stealthy and stealthy hyperuniform ones exhibit strong anticorrelations in their Voronoi cell areas, manifested as the negative values of $C_{00}(r)$. Such anticorrelations

of Voronoi cell areas indicate that in these networks large Voronoi cells are accompanied with small cells (and vice versa), which in turn suppresses large-scale area fluctuations to achieve hyperuniformity. The observed anticorrelations are consistent with the previous analysis of the hyperuniform MRJ sphere packings in 3D [44]. Our results indicate that the correlation functions $C_{00}(r)$, which encode nonlocal pair-correlation information of Voronoi cells, can qualitatively distinguish the antihyperuniform, nonhyperuniform, and hyperuniform Voronoi networks considered here.

IV. CONCLUSIONS AND DISCUSSION

In this work, we presented a comprehensive analysis of the structural properties of large two-dimensional nonhyperuniform and hyperuniform networks, derived from the Voronoi tessellations of antihyperuniform hyperplane intersection process, nonhyperuniform Poisson process, nonhyperuniform RSA saturated packings, and both non-stealthy and stealthy hyperuniform point processes. Specifically, we carried out an extensive study of the Voronoi-cell area distribution of each of the networks using multiple metrics that characterize the distribution, including the first four cumulants, i.e., average $\bar{A}$, variance σ_A^2, skewness γ_1 and excess kurtosis γ_2. We showed that the antihyperuniform HIP distribution is far from Gaussian, as evidenced by a high skewness ($\gamma_1 = 3.16$) and large positive excess kurtosis ($\gamma_2 = 16.2$). The nonhyperuniform Poisson (with $\gamma_1 = 1.07$ and $\gamma_2 = 1.79$) and non-stealthy hyperuniform (with $\gamma_1 = 0.257$ and $\gamma_2 = 0.0217$) distributions are Gaussian-like distributions as they exhibit a small but positive skewness and excess kurtosis. The nonhyperuniform RSA (with $\gamma_1 = 0.450$ and $\gamma_2 = -0.0384$) and the highest stealthy hyperuniform distributions (with $\gamma_1 = 0.0272$ and $\gamma_2 = -0.0626$) are also non-Gaussian because of their low skewness and negative excess kurtosis, which is diametrically opposite non-Gaussian behavior of the HIP. The fact that the cell-area distributions of large, finite-sized RSA and stealthy hyperuniform networks (e.g., with $N \approx 10,000$ nodes) are narrower, have larger peaks, and smaller tails than a Gaussian distribution implies that in the thermodynamic limit the distributions should exhibit compact support, which is consistent with the previous theoretical considerations [60].

Moreover, we computed the Voronoi-area correlation functions $C_{00}(r)$ for the networks, which quantify the correlations of areas of two Voronoi cells separated by distance r. We found that the antihyperuniform HIP networks possess a slowly decaying $C_{00}(r)$ with large positive values, while the nonhyperuniform Poisson and RSA network possess positive and fast decaying $C_{00}(r)$. In contrast, we observed strong anticorrelations in $C_{00}(r)$ (i.e., negative values) for the hyperuniform networks, including both the non-stealthy and stealthy ones. Such anticorrelations are realized by accompanying large Voronoi cells with small cells (and vice versa) in the systems, which suppress large-scale area fluctuations to achieve hyperuniformity. These results indicate that $C_{00}(r)$ qualitatively distinguishes the antihyperuniform, nonhyperuniform and hyperuniform Voronoi networks considered here.

Our work here marks an attempt toward the generalization of the analysis of hyperuniform point configurations, two-phase media, and random fields to hyperuniform network systems. In general, a network can encode the complex interactions between individual elements of a system [46,83–87] by building a topological map of the system that may or may not encode geometrical distance information. Networks have been used to model complex systems in many different fields, and their analysis has led to many fascinating discoveries [46,54–56,88–97]. In our future work, we will further explore the existing network tools and develop new ones to investigate hyperuniform network systems.

ACKNOWLEDGMENT

We thank Adilson Motter for valuable discussions. This work was supported by the Army Research Office under Cooperative Agreement Number W911NF-22-2-0103.

[1] S. Torquato and F. H. Stillinger, Local density fluctuations, hyperuniformity, and order metrics, Phys. Rev. E **68**, 041113 (2003).

[2] S. Torquato, Hyperuniform states of matter, Phys. Rep. **745**, 1 (2018).

[3] A. Donev, F. H. Stillinger, and S. Torquato, Unexpected density fluctuations in jammed disordered sphere packings, Phys. Rev. Lett. **95**, 090604 (2005).

[4] C. E. Zachary and S. Torquato, Hyperuniformity in point patterns and two-phase random heterogeneous media, J. Stat. Mech. (2009) P12015.

[5] Y. Jiao, T. Lau, H. Hatzikirou, M. Meyer-Hermann, J. C. Corbo, and S. Torquato, Avian photoreceptor patterns represent a disordered hyperuniform solution to a multiscale packing problem, Phys. Rev. E **89**, 022721 (2014).

[6] S. Torquato, Hyperuniformity and its generalizations, Phys. Rev. E **94**, 022122 (2016).

[7] O. Leseur, R. Pierrat, and R. Carminati, High-density hyperuniform materials can be transparent, Optica **3**, 763 (2016).

[8] D. Hexner and D. Levine, Noise, diffusion, and hyperuniformity, Phys. Rev. Lett. **118**, 020601 (2017).

[9] D. Hexner, P. M. Chaikin, and D. Levine, Enhanced hyperuniformity from random reorganization, Proc. Natl. Acad. Sci. USA **114**, 4294 (2017).

[10] J. H. Weijs and D. Bartolo, Mixing by unstirring: Hyperuniform dispersion of interacting particles upon chaotic advection, Phys. Rev. Lett. **119**, 048002 (2017).

[11] S. Torquato, G. Zhang, and M. De Courcy-Ireland, Hidden multiscale order in the primes, J. Phys. A: Math. Theor. **52**, 135002 (2019).

[12] D. Chen, X. Jiang, D. Wang, H. Zhuang, and Y. Jiao, Multi-hyperuniform long-range order in medium-entropy alloys, Acta Mater. **246**, 118678 (2023).

[13] Y. Zheng, L. Liu, H. Nan, Z.-X. Shen, G. Zhang, D. Chen, L. He, W. Xu, M. Chen, Y. Jiao, and H. Zhuang, Disordered hyperuniformity in two-dimensional amorphous silica, Sci. Adv. **6**, eaba0826 (2020).

[14] M. Salvalaglio, M. Bouabdellaoui, M. Bollani, A. Benali, L. Favre, J.-B. Claude, J. Wenger, P. de Anna, F. Intonti, A. Voigt *et al.*, Hyperuniform monocrystalline structures by spinodal solid-state dewetting, Phys. Rev. Lett. **125**, 126101 (2020).

[15] D. Chen, Y. Zheng, L. Liu, G. Zhang, M. Chen, Y. Jiao, and H. Zhuang, Stone-wales defects preserve hyperuniformity in amorphous two-dimensional networks, Proc. Natl. Acad. Sci. USA **118**, e2016862118 (2021).

[16] S. Sakai, R. Arita, and T. Ohtsuki, Quantum phase transition between hyperuniform density distributions, Phys. Rev. Res. **4**, 033241 (2022).

[17] J. Puig, F. Elías, J. Aragón Sánchez, R. Cortés Maldonado, G. Rumi, G. Nieva, P. Pedrazzini, A. B. Kolton, and Y. Fasano, Anisotropic suppression of hyperuniformity of elastic systems in media with planar disorder, Commun. Mater. **3**, 32 (2022).

[18] Z. Ge, The hidden order of turing patterns in arid and semi-arid vegetation ecosystems, Proc. Natl. Acad. Sci. USA **120**, e2306514120 (2023).

[19] O. H. E. Philcox and S. Torquato, Disordered heterogeneous universe: Galaxy distribution and clustering across length scales, Phys. Rev. X **13**, 011038 (2023).

[20] H. Zhang, X. Wang, J. Zhang, H.-B. Yu, and J. F. Douglas, Approach to hyperuniformity in a metallic glass-forming material exhibiting a fragile to strong glass transition, Eur. Phys. J. E **46**, 50 (2023).

[21] S. Wilken, R. E. Guerra, D. Levine, and P. M. Chaikin, Random close packing as a dynamical phase transition, Phys. Rev. Lett. **127**, 038002 (2021).

[22] Y. Liu, D. Chen, J. Tian, W. Xu, and Y. Jiao, Universal hyperuniform organization in looped leaf vein networks, Phys. Rev. Lett. **133**, 028401 (2024).

[23] J. A. Sánchez, R. C. Maldonado, M. L. Amigó, G. Nieva, A. Kolton, and Y. Fasano, Disordered hyperuniform vortex matter with rhombic distortions in fese at low fields, Phys. Rev. B **107**, 094508 (2023).

[24] M. Florescu, S. Torquato, and P. J. Steinhardt, Designer disordered materials with large, complete photonic band gaps, Proc. Natl. Acad. Sci. USA **106**, 20658 (2009).

[25] W. Man, M. Florescu, E. P. Williamson, Y. He, S. R. Hashemizad, B. Y. C. Leung, D. R. Liner, S. Torquato, P. M. Chaikin, and P. J. Steinhardt, Isotropic band gaps and freeform waveguides observed in hyperuniform disordered photonic solids, Proc. Natl. Acad. Sci. USA **110**, 15886 (2013).

[26] M. Florescu, P. J. Steinhardt, and S. Torquato, Optical cavities and waveguides in hyperuniform disordered photonic solids, Phys. Rev. B **87**, 165116 (2013).

[27] J. H. Weijs, R. Jeanneret, R. Dreyfus, and D. Bartolo, Emergent hyperuniformity in periodically driven emulsions, Phys. Rev. Lett. **115**, 108301 (2015).

[28] Y. Xu, S. Chen, P.-E. Chen, W. Xu, and Y. Jiao, Microstructure and mechanical properties of hyperuniform heterogeneous materials, Phys. Rev. E **96**, 043301 (2017).

[29] B.-Y. Wu, X.-Q. Sheng, and Y. Hao, Effective media properties of hyperuniform disordered composite materials, PLoS ONE **12**, e0185921 (2017).

[30] G. Rumi, J. A. Sánchez, F. Elías, R. C. Maldonado, J. Puig, N. R. C. Bolecek, G. Nieva, M. Konczykowski, Y. Fasano, and A. B. Kolton, Hyperuniform vortex patterns at the surface of type-ii superconductors, Phys. Rev. Res. **1**, 033057 (2019).

[31] Q.-L. Lei and R. Ni, Hydrodynamics of random-organizing hyperuniform fluids, Proc. Natl. Acad. Sci. USA **116**, 22983 (2019).

[32] H. Zhang, H. Chu, H. Giddens, W. Wu, and Y. Hao, Experimental demonstration of luneburg lens based on hyperuniform disordered media, Appl. Phys. Lett. **114**, 053507 (2019).

[33] É. Chéron, S. Félix, J.-P. Groby, V. Pagneux, and V. Romero-García, Wave transport in stealth hyperuniform materials: The diffusive regime and beyond, Appl. Phys. Lett. **121**, 061702 (2022).

[34] N. Tavakoli, R. Spalding, A. Lambertz, P. Koppejan, G. Gkantzounis, C. Wan, R. Rohrich, E. Kontoleta, A. F. Koenderink, R. Sapienza *et al.*, Over 65% sunlight absorption in a 1 μm Si Slab with hyperuniform texture, ACS Photonics **9**, 1206 (2022).

[35] N. Granchi, R. Spalding, M. Lodde, M. Petruzzella, F. W. Otten, A. Fiore, F. Intonti, R. Sapienza, M. Florescu, and M. Gurioli, Near-field investigation of luminescent hyperuniform disordered materials, Adv. Opt. Mater. **10**, 2102565 (2022).

[36] H. Tang, Z. Hao, Y. Liu, Y. Tian, H. Niu, and J. Zang, Soft and disordered hyperuniform elastic metamaterials for highly efficient vibration concentration, Nat. Sci. Rev. **9**, nwab133 (2022).

[37] D. Chen, Y. Liu, Y. Zheng, H. Zhuang, M. Chen, and Y. Jiao, Disordered hyperuniform quasi-one-dimensional materials, Phys. Rev. B **106**, 235427 (2022).

[38] D. Chen, H. Zhuang, M. Chen, P. Y. Huang, V. Vlcek, and Y. Jiao, Disordered hyperuniform solid state materials, Appl. Phys. Rev. **10**, 021310 (2023).

[39] H. Zhuang, D. Chen, L. Liu, D. Keeney, G. Zhang, and Y. Jiao, Vibrational properties of disordered stealthy hyperuniform 1D atomic chains, J. Phys.: Condens. Matter **36**, 285703 (2024).

[40] S. Torquato, G. Zhang, and F. H. Stillinger, Ensemble theory for stealthy hyperuniform disordered ground states, Phys. Rev. X **5**, 021020 (2015).

[41] G. Zhang, F. H. Stillinger, and S. Torquato, Ground states of stealthy hyperuniform potentials. I. Entropically favored configurations, Phys. Rev. E **92**, 022119 (2015).

[42] G. Zhang, F. H. Stillinger, and S. Torquato, Ground states of stealthy hyperuniform potentials: II. Stacked-slider phases, Phys. Rev. E **92**, 022120 (2015).

[43] G. Zhang, F. H. Stillinger, and S. Torquato, Can exotic disordered stealthy particle configurations tolerate arbitrarily large holes? Soft Matter **13**, 6197 (2017).

[44] M. A. Klatt and S. Torquato, Characterization of maximally random jammed sphere packings: Voronoi correlation functions, Phys. Rev. E **90**, 052120 (2014).

[45] M. Salvalaglio, D. J. Skinner, J. Dunkel, and A. Voigt, Persistent homology and topological statistics of hyperuniform point clouds, Phys. Rev. Res. **6**, 023107 (2024).

[46] M. Barthélemy, Spatial networks, Phys. Rep. **499**, 1 (2011).

[47] L. Daqing, K. Kosmidis, A. Bunde, and S. Havlin, Dimension of spatially embedded networks, Nat. Phys. **7**, 481 (2011).

[48] F. Aurenhammer, Voronoi diagrams: A survey of a fundamental geometric data structure, ACM Comput. Surv. **23**, 345 (1991).

[49] S. Torquato, *Random Heterogeneous Materials: Microstructure and Macroscopic Properties* (Springer-Verlag, New York, 2002).

[50] E. A. Lazar, J. Lu, and C. H. Rycroft, Voronoi cell analysis: The shapes of particle systems, Am. J. Phys. **90**, 469 (2022).

[51] S.-H. Yook, H. Jeong, and A.-L. Barabási, Modeling the internet's large-scale topology, Proc. Natl. Acad. Sci. USA **99**, 13382 (2002).
[52] E. Bullmore and O. Sporns, Complex brain networks: graph theoretical analysis of structural and functional systems, Nat. Rev. Neurosci. **10**, 186 (2009).
[53] R. Z. Farahani, E. Miandoabchi, W. Y. Szeto, and H. Rashidi, A review of urban transportation network design problems, Eur. J. Oper. Res. **229**, 281 (2013).
[54] L. Papadopoulos, M. A. Porter, K. E. Daniels, and D. S. Bassett, Network analysis of particles and grains, J. Complex Networks **6**, 485 (2018).
[55] Q. Duchemin and Y. De Castro, Random geometric graph: Some recent developments and perspectives, in *High Dimensional Probability IX*, edited by R. Adamczak, N.l Gozlan, K. Lounici, and M. Madiman (Springer International Publishing, Cham, 2023), pp. 347–392.
[56] M. Penrose, *Random Geometric Graphs* (Oxford University Press, Oxford, 2003).
[57] G. Zhang and S. Torquato, Precise algorithm to generate random sequential addition of hard hyperspheres at saturation, Phys. Rev. E **88**, 053312 (2013).
[58] G. Zhang, F. H. Stillinger, and S. Torquato, Transport, geometrical, and topological properties of stealthy disordered hyperuniform two-phase systems, J. Chem. Phys. **145**, 244109 (2016).
[59] S. Ghosh and J. L. Lebowitz, Generalized stealthy hyperuniform processes: Maximal rigidity and the bounded holes conjecture, Commun. Math. Phys. **363**, 97 (2018).
[60] S. Torquato, J. Kim, and M. A. Klatt, Local number fluctuations in hyperuniform and nonhyperuniform systems: Higher-order moments and distribution functions, Phys. Rev. X **11**, 021028 (2021).
[61] H. Wang and S. Torquato, Equilibrium states corresponding to targeted hyperuniform nonequilibrium pair statistics, Soft Matter **19**, 550 (2023).
[62] S. N. Chiu, D. Stoyan, W. S. Kendall, and J. Mecke, *Stochastic Geometry and Its Applications*, 3rd ed., edited by S. N. Chiu, D. Stoyan, W. S. Kendall, and J. Mecke, Wiley Series in Probability and Statistics (Wiley-Blackwell, Hoboken, NJ, 2013).
[63] S. Torquato, O. U. Uche, and F. H. Stillinger, Random sequential addition of hard spheres in high euclidean dimensions, Phys. Rev. E **74**, 061308 (2006).
[64] H. Wang and S. Torquato, Designer pair statistics of disordered many-particle systems with novel properties, J. Chem. Phys. **160**, 044911 (2024).
[65] O. U. Uche, F. H. Stillinger, and S. Torquato, Constraints on collective density variables: Two dimensions, Phys. Rev. E **70**, 046122 (2004).
[66] R. D. Batten, F. H. Stillinger, and S. Torquato, Classical disordered ground states: Super-ideal gases and stealth and equi-luminous materials, J. Appl. Phys. **104**, 033504 (2008).
[67] S. Torquato, Random heterogeneous materials: microstructure and macroscopic properties, Appl. Mech. Rev. **55**, B62 (2002).
[68] E. C. Oğuz, J. E. S. Socolar, P. J. Steinhardt, and S. Torquato, Hyperuniformity of quasicrystals, Phys. Rev. B **95**, 054119 (2017).
[69] D. Chen and S. Torquato, Designing disordered hyperuniform two-phase materials with novel physical properties, Acta Mater. **142**, 152 (2018).
[70] G. Zhang, F. H. Stillinger, and S. Torquato, Classical many-particle systems with unique disordered ground states, Phys. Rev. E **96**, 042146 (2017).
[71] C. E. Zachary, Y. Jiao, and S. Torquato, Hyperuniform long-range correlations are a signature of disordered jammed hard-particle packings, Phys. Rev. Lett. **106**, 178001 (2011).
[72] Y. Jiao and S. Torquato, Maximally random jammed packings of platonic solids: Hyperuniform long-range correlations and isostaticity, Phys. Rev. E **84**, 041309 (2011).
[73] C. E. Zachary, Y. Jiao, and S. Torquato, Hyperuniformity, quasi-long-range correlations, and void-space constraints in maximally random jammed particle packings. I. Polydisperse spheres, Phys. Rev. E **83**, 051308 (2011).
[74] C. E. Zachary, Y. Jiao, and S. Torquato, Hyperuniformity, quasi-long-range correlations, and void-space constraints in maximally random jammed particle packings. II. Anisotropy in particle shape, Phys. Rev. E **83**, 051309 (2011).
[75] C. E. Zachary and S. Torquato, Anomalous local coordination, density fluctuations, and void statistics in disordered hyperuniform many-particle ground states, Phys. Rev. E **83**, 051133 (2011).
[76] D. Hexner and D. Levine, Hyperuniformity of critical absorbing states, Phys. Rev. Lett. **114**, 110602 (2015).
[77] J. Kim and S. Torquato, Effect of imperfections on the hyperuniformity of many-body systems, Phys. Rev. B **97**, 054105 (2018).
[78] P. N. Andrade and M. A. Fortes, Distribution of cell volumes in a voronoi partition, Philos. Mag. B **58**, 671 (1988).
[79] V. Senthil Kumar and V. Kumaran, Voronoi cell volume distribution and configurational entropy of hard-spheres, J. Chem. Phys. **123**, 114501 (2005).
[80] J.-S. Ferenc and Z. Néda, On the size distribution of poisson voronoi cells, Physica A **385**, 518 (2007).
[81] J. B. Hough, M. Krishnapur, Y. Peres, and B. Virág, *Zeros of Gaussian Analytic Functions and Determinantal Point Processes*, University Lecture Series (American Mathematical Society, Providence, RI, 2009).
[82] S. Ghosh and A. Nishry, Gaussian complex zeros on the hole event: The emergence of a forbidden region, Commun. Pure Appl. Math. **72**, 3 (2019).
[83] B. Bollobás, Graph theory: An introductory course, The Mathematical Gazette **64**, 217 (1980).
[84] M. E. J. Newman, The structure and function of complex networks, SIAM Rev. **45**, 167 (2003).
[85] D. J. Watts, The new science of networks, Annual Review of Sociology **30**, 243 (2004).
[86] A.-L. Barabási and M. Pósfai, *Network science* (Cambridge University Press, Cambridge, 2016).
[87] M. Newman, *Networks* (Oxford University Press, 2018).
[88] Y. Jiao and S. Torquato, Quantitative characterization of the microstructure and transport properties of biopolymer networks, Phys. Biol. **9**, 036009 (2012).
[89] S. Wasserman and K. Faust, *Social Network Analysis: Methods and Applications*, Structural Analysis in the Social Sciences (Cambridge University Press, Cambridge, 1994).
[90] R. Milo, S. Shen-Orr, S. Itzkovitz, N. Kashtan, D. Chklovskii, and U. Alon, Network motifs: Simple building blocks of complex networks, Science **298**, 824 (2002).
[91] E. Alm and A. P. Arkin, Biological networks, Curr. Opin. Struct. Biol. **13**, 193 (2003).

[92] J. J. Tyson, K. C. Chen, and B. Novak, Sniffers, buzzers, toggles and blinkers: Dynamics of regulatory and signaling pathways in the cell, Curr. Opin. Cell Biol. **15**, 221 (2003).

[93] U. Alon, *An Introduction to Systems Biology: Design Principles of Biological Circuits* (CRC Press, Boca Raton, FL, 2006).

[94] A. Vespignani, Modelling dynamical processes in complex socio-technical systems, Nat. Phys. **8**, 32 (2012).

[95] R. Albert, B. DasGupta, and N. Mobasheri, Topological implications of negative curvature for biological and social networks, Phys. Rev. E **89**, 032811 (2014).

[96] P. Woerner, A. G. Nair, K. Taira, and W. S. Oates, Sparsification of long range force networks for molecular dynamics simulations, PLOS ONE **14**, e0213262 (2019).

[97] M. Aykol, V. I. Hegde, L. Hung, S. Suram, P. Herring, C. Wolverton, and J. S. Hummelshøj, Network analysis of synthesizable materials discovery, Nat. Commun. **10**, 2018 (2019).